Chapter 12
Optimization of Multi-stage Cooling System's Performance for Hydrogen Fueled Scramjet

Pourya Seyedmatin, Mohammad Ebadollahi, Mojtaba Bezaatpour, and Majid Amidpour

Abstract Hydrogen fueled scramjet is an interesting choice to be used as engine of aerospace vehicles because of its high specific impulse. The most important challenge in scramjet engine technology is the thermal management of them. Due to high temperature of combustion, a competent cooling system which is able to recover the waste energy is needed. The multi-stage open cooling cycle was proposed as appropriate choice by many recent studies. In the present study, the optimization of a novel multi-stage cooling system for hydrogen fueled scramjets is conducted in which the waste heat of scramjet is recovered to produce power and electricity. The optimization process has been done through a thermodynamic zero dimensional analysis. The waste heat of scramjet is used as main heat source of the system. The present study results declare that the energy and exergy efficiencies of the system is improved by 49.24% and 45.98% by optimizing the M-OCC, respectively. In both performance criterion of the system a huge sensible improvement is observed by accomplished optimization.

Keywords Optimization · Scramjet · Hydrogen production · Thermodynamic analysis · Mach number

Nomenclature

Symbols

c_p Special heat magnitude ($kJ \cdot kg^{-1} \cdot K^{-1}$)

P. Seyedmatin
Tarbiat Modares University of Tehran, Tehran, Iran

M. Ebadollahi · M. Amidpour (✉)
Khajeh Nasir Toosi University of Technology, Tehran, Iran
e-mail: amidpour@kntu.ac.ir

M. Bezaatpour
Sahand University of Technology, Tabriz, Iran

M. Amidpour et al. (eds.), *Synergy Development in Renewables Assisted Multi-carrier Systems*, Green Energy and Technology, https://doi.org/10.1007/978-3-030-90720-4_12

D	Thickness of memberane (μm)
E	Electrical energy (kJ)
ex	The exergy rate (kW/kg)
$\dot{E}x$	The energy rate (kW)
F	Faraday constant (C/mol)
G	Gibbs free energy ($\mathrm{kJ \cdot kmol^{-1}}$)
H	Molar specific enthalpy ($\mathrm{kJ \cdot kmol^{-1}}$)
h	Mass specific enthalpy ($\mathrm{kJ \cdot kg^{-1}}$)
J	Density of current ($\mathrm{A.m^{-2}}$)
J_a^{ref}	Anode pre-exponential factor ($\mathrm{A \cdot m^{-2}}$)
J_c^{ref}	Cathode pre-exponential factor ($\mathrm{A \cdot m^{-2}}$)
J_i^{ref}	Pre-exponential factor ($\mathrm{A \cdot m^{-2}}$)
LHV	Lower heating value ($\mathrm{kJ \cdot kg^{-1}}$)
$\dot{m}$	Mass flow rate ($\mathrm{kg \cdot s^{-1}}$)
Ma	Mach number
$\dot{N}$	Molar mass flow rate ($\mathrm{kmol \cdot s^{-1}}$)
P	Pressure (MPa)
Q	Heat energy (kJ)
$\dot{Q}$	The rate of heat transfer (kW)
R	Ohmic resistance of PEM (Ω)
Re	Reynolds number
T	Temperature (K)
V_0	Reversible potential (V)
$V_{act,a}$	Anode activation over-potential (V)
$V_{act,c}$	Cathode activation over-potential (V)
V_0	Reversible potential (V)
V	Electrical potential (V)
w	Specific power per mass unit (MW/kg)
$\dot{W}$	Electricity rate (kW)
x	Membrane distance (m

Greek Symbols

η	Efficiency (%)
$\varnothing$	Fuel equivalence ratio
δ	Ratio of multiplication
ϕ	Ratio of reduction
ρ	Density ($\mathrm{kg.m^{-3}}$)
γ	Heat capacity ratio
K	Air heat capacity ratio
π	Pressure ratio

Acronyms

EES	Engineering Equation Solver
HE	Heat exchanger
OCC	Open cooling cycle
PEM	Proton exchange membrane
RCC	Regenerative cooling cycle

Superscripts and Subscripts

a	Anode
act,a	Anode activation
act,c	Cathode activation
ave	Average
c	Cathode
CP	Cooling passage
cr	Critical
D	Destruction
en	Energy
ex	Exergy
F	Fuel
int	Intermediate
in	Inlet
is	Isentropic
j	Jth stage
KN	Kinetic
net	Net value
out	Outlet
P	Product
p	Pump
scr	Scramjet
t	Turbine
v	Vapor
1,2,…	Cycle locations
0	Dead state
A,B,..	Scramjet states

12.1 Introduction

Aerospace scientists have noticed the air-breathing propulsion vehicles, since several decades ago. Supersonic combustion chambers (scramjets) have great ability in high speed hence have acquired high level of recent research interest in all over the world [1, 2]. Due to high fuel impulse, scramjets can be considered as one of economic choice in long-distance flights [3]. However, scramjets are not very appropriate for accelerating missions since their net thrust is lower than a rocket [4]. Whereas, scramjet technology face up to many challenges such cooling management of high working temperature, onboard fuel storage restriction, flight condition sustainability etc. Accordingly, prevailing over these challenges can be purpose of developed research centers.

High heat flux level in scramjet combustion chambers demands a reliable cooling system. Heat flux range of 0.5–2.5 MW per unit of area in working temperature of 500–2000 K for Mach number of 8 flight condition is reported [5]. Due to such high temperature, even the most developed composite materials cannot withstand a work properly [6]. Regenerative cooling systems (RCC) especially open cooling cycle (OCC) is introduced as one of the most efficient and feasible solution encountering heat management challenge. Utilizing the high heat absorption of hydrogen to cool down the scramjet is the innovative point of this method. Over-temperature of the wall in the scramjet systems is a crucial phenomenon through the cooling process which can be avoided by preheating of the fuel before entering the cooling channel [7]. Thus, an appropriate cooling treatment prevents the heat transfer deterioration at the entrance region. This process may be repeated in various times that is called multi-OCC (M-OCC). OCC is also applicable to both hydrocarbon and hydrogen-fueled scramjet engines.

The ancillary set-ups, including circuit measuring, fuel injection, and tracking controller set-ups on aircrafts and aerospace vehicles need a definite deal of electrical energy. Thus, for such a high speed enormous vehicles, it is completely important to provide an energy recovery set-up to address its surplus electricity need [8]. In recent years, recovering energy and implementing energy-saving methods for producing power, useful products and other required commodities have been utilized in numerous energy conversion systems [9]. Consequently, co-production systems are introduced as the most efficient and pragmatic solutions for energy recovery purposes when low-quality heat resources (such as waste heat) are pondered [10, 11]. Using co-production systems render the feasibility of producing other useful forms of energies such as heating, cooling, purified water and hydrogen alongside the power production [12–14]. Co-production (also known as co-generation) systems have higher energy efficiency and low exergy destruction than the single-production systems under a same condition, as shown by Onovwiona and Ugursl [15]. Dincer et al. [16] carried out a thermodynamic study of a high degree set-up electrolysis (HDSE) for cogeneration of H_2 and electricity, including a solar tower, a Brayton system, a Rankine system, and an organic Rankine system. Based on the results, the total efficiencies. Ghaebi et al. [17] recommended two novel combined cycles for

electricity and H_2 co-production using huge value of wasted heat of the city gas post (CGP) regulators in which the high pressure NG is decreased to an acceptable pressure for consumption. These set-ups are integrated by a combination of a Rankine system (RS) and CGP system as well as an absorption power system (APS) as an alternative electricity unit. In both systems, PEM electrolyzer is utilized to generate hydrogen. The power sub-cycle is actuated by waste heat of CGP and PEM is operated by a fair segment of net output electricity. An executive and comparative 4E (energy, exergy, economy and environment) analysis of both systems have been fulfilled. The outcomes of assessment have demonstrated 6.868 and 6.351 kg/h hydrogen production as well as 8.571 and 7.618 MW electricity generation for the CGP-RS and CGP-APS set-ups, correspondingly. The exergy destruction study has demonstrated that the generator of system has introduced as the highest exergy destructive component (in both systems). Li and Wang [5] have performed a theoretical study on producing power from the waste energy of scramjet. In their study, a thermoelectrical generator (TEG) is assimilated with a regenerative cooling cycle of scramjet engine for power production. The results of this study revealed power production of 61.69 kW and exergy efficiency of about 22% for fuel flow rate of 0.4 kg/s. And a parametric analysis which has been accomplished in their investigation denoted that the pressure ratio of turbine has a significant effect on the exergy efficiency.

Hydrogen has higher-ranking properties compared to all kinds of carbon based fuels such as substantial flame stability for combustion and high ignitability. These intrinsic profits nowadays have captured a great attention in recent studies of H_2-fueled scramjet engines [7, 10, 18]. H_2 production process c is performed by biomass conversion water splitting or steam methane reforming. Splitting water is a thermochemical process which is called electrolysis. There are three conventional forms for electrolyzing process, consist of the alkaline, oxidation of solid, and proton exchange membrane (PEM) electrolysis. Hydrogen generation by PEM electrolysis has several benefits especially in renewable-based procedures, including: being compact, low environmental effect, zero hazardous chemicals and extremely pure hydrogen [19]. PEM is the most widespread procedure of hydrogen production in energy set-ups with low grade energy sources because of its high compatibility with these systems and is introduced as the commendable hydrogen production method for future utilities accordingly [20, 21]. Marangio et al. [22] presented a model for theoretical study of the PEM cells in which a complicated pattern of Ohmic losses in electrodes and membrane. They have validated the presented model using available experimental data. In the other study presented by Ahmadi et al. [23], a PEM electrolyzer which is actuated by solar energy, has been assimilated with an OHEC (ocean heat energy conversion) system to extract H_2. Energy and exergy assessment have been performed in the recommended model and it is concluded that the extracted hydrogen rate is 1.2 kg/h with exergy and thermodynamic efficiencies of 23% and 3.6%, respectively.

The importance of thermal management of the scramjet and its effects on operation of this hypersonic vehicle has drawn attention of many researches about it in more recent years. The M-OCC is known as one of the most feasible system for cooling of scramjet engines. On the other hand, some studies have tried to examine the exergy aspect of utilizing this kind of cooling system for co-production aims such

as a limited exergy based study conducted by Li and Wang. Despite all efforts to study and outstrip these cooling systems and conducting thermodynamic analysis of these systems, the lack of an exclusive thermodynamic and exergy analysis of the M-OCC and investigating the effects of multi-expansion process is also indispensable. Moreover, no thoroughgoing investigation for producing electricity and hydrogen from waste heat of scramjet via PEM electrolyzer is presented up to yet.

The aim of present work is to advance a novel multi-stage OCC in order to produce electricity and hydrogen and cooling the scramjet engine as well. Additionally, a thoroughgoing study on multi-expansion effects is accomplished from thermodynamic standpoint. In the proposed set-up, the PEM is driven by a portion of net output power the cooling cycle, whilst the waste heat of scramjet is pondered as the heat source of the multi cooling cycle.

12.2 System Expression

Figure 12.1 shows a comprehensive illustration of system layout. Two prominent systems, Power and PEM electrolyzer cycles, are operating in this system. Hydrogen as working flow, is streamed through scramjet cooling pass entry by pump (state 2). Coolant absorbs the combustion chamber heat and changes to superhot gas quickly. Afterwards, the superhot hydrogen gets on the turbine number 1 (state 3). By entering to the turbine the hydrogen as working fluid not only produce electric power but also the temperature decreases to T_4. Hydrogen produced power, by circulating in turbine, and now is cooled down. Thus it is again ready to absorb the heat and cool down through the second cooling passage and turbine number 2, respectively. This

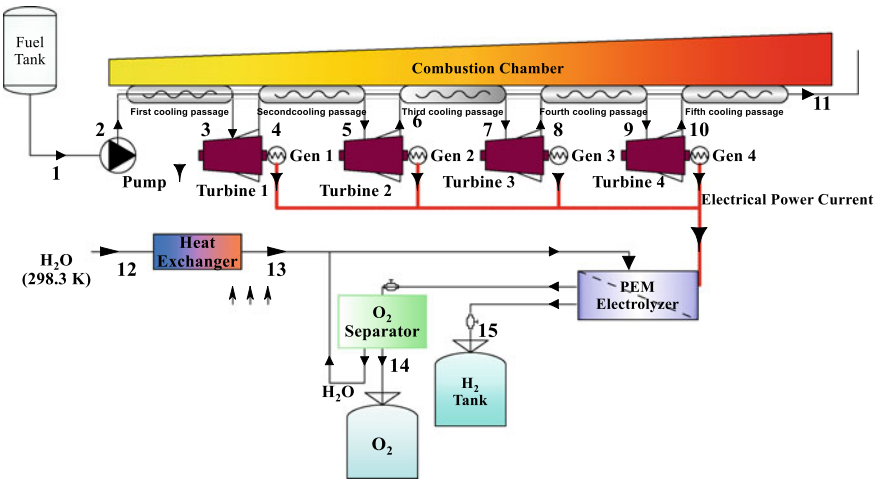

Fig. 12.1 Simple schematics of proposed system

process of chilling the scramjet wall down and expanding through turbine to extract electricity from the heated coolant continues two times again in order to attain a high performance. Finally hydrogen enters to the combustion chamber of scramjet as fuel after streaming into last cooling passage to close the power sub-cycle.

Electricity and heat energy are two main inputs of PEM electrolyzer to produce hydrogen. Some portion of produced electricity in the power sub-cycle supplies the electricity need of PEM and high heat flux of scramjet meets heat needs of PEM. A simple electrolyzing process of water separation occurs in the PEM. Electric voltage difference make to anode and cathode sides. Hydrogen is produced in cathode side then is storied in a special tank (state 15). In the anode side the separated oxygen is accumulated and transferred to a storage tank (state 16). The surplus water is recirculated to the PEM and closes the PEM sub-cycle.

12.3 Methodology and Assumptions

12.3.1 Considered Suppositions

Some of the main assumptions of the suggested system are made as following [24–28]:

- Mathematical modeling is zero dimensional steady state
- Specific heat is considered constant.
- After the first cooling passage, the coolant is assumed perfect gas.
- Any energy and pressure drops are not considered through joints and transfer lines.
- Any losses is not considered by heat transfer process in the turbine.
- 298 K and 0.101 MPa are reference temperature and presure, respectively.
- Any energy losses is not considered through PEM electrolyzer.

12.3.2 The Mathematic Simulation of Scramjet

The thermodynamic analysis based modeling of scramjet is conducted in present modeling. Therefore, two main parameters consisting of the scramjet's entry pressure ratio (π_{in}) and fuel equivalence ratio are needed to evaluate the average temperature of scramjet combustion chamber wall. The mean wall combustor temperature is calculated by averaging TD and TC, which means the outlet and inlet combustor temperatures (Fig. 12.2):

$$T_{ave} = \frac{T_c + T_D}{2} \tag{12.1}$$

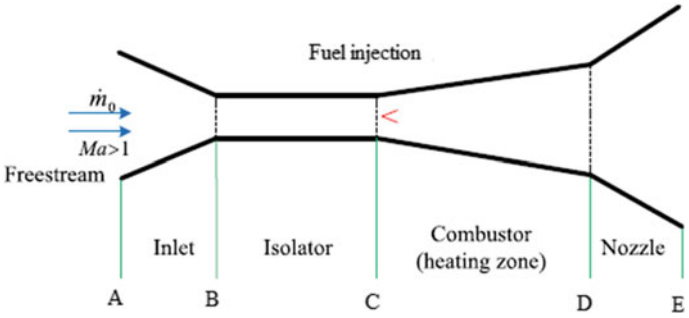

Fig. 12.2 Ideal scramjet Schematic condition

Figure 12.2 indicates a schematic plot of an ideal scramjet, which includes four prominent zones of inlet, nozzle, isolator, and combustor. The combustor is supplied by hydrogen.

12.3.3 Cycle Analysis for the Scramjet Engine Modeling

As demonstrated in Fig. 12.3, the ideal scramjet system is drawn on a T-s plot. A-C process indicates the adiabatic compression from the static temperature to the combustor inlet temperature. A-B and B-C indicate air compression in the enter section and isolator. C-D shows the energy receiving operation in to combustor, performing at a consistent static pressure. Process D-E occurs isentropically in the nozzle. Also, process E-A is only an unreal constant static pressure event. Based on

Fig. 12.3 T-s diagram of an ideal scramjet system

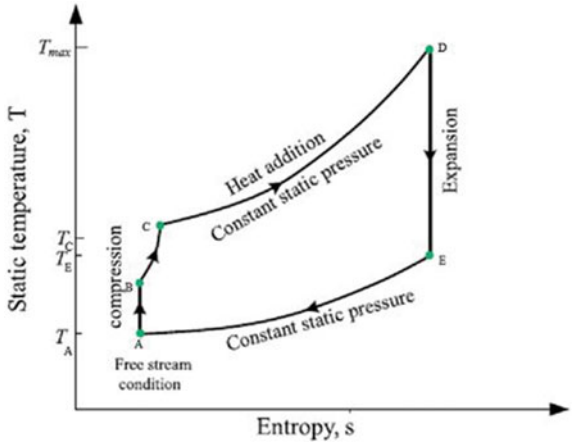

energy conversion principle, heat is wasted from nozzle outlet to the atmosphere at D-A process. The Three main sectors in scramjet modeling are described extensively.

12.3.3.1 Compression Process

The amount of compression in the scramjet inlet section defines as inlet pressure ratio (π_{in}). At cruise situations, the freestream circumstances (P_{tA}, T_{tA} and Ma_A) are expressed. However, the steady flow through the inlet compression part may be written as below [29, 30]:

$$P_{tB} = P_{tA} \tag{12.2}$$

$$T_{tB} = T_{tA} \tag{12.3}$$

$$Ma_B = \sqrt{\left[\left(\frac{P_{tA}}{\pi_{in} P_A}\right)^{(k-1/k)}\right] \Big/ \left(\frac{k-1}{2}\right)} \tag{12.4}$$

Also, k is the specific heat capacity ratio of air.

The isolator compression is followed by a shock train. The empirical relations are described by Billig et al. [31, 32]:

$$\frac{L}{H} = \frac{\left[50\left(\frac{P_C}{P_B} - 1\right)^2 + 170\left(\frac{P_C}{P_B} - 1\right)^2\right]}{\left(Ma_1^2 - 1\right)} \cdot \frac{\sqrt{\theta/H}}{\sqrt[4]{Re_\theta}} \tag{12.5}$$

where, Re_θ is the inlet Reynolds number, θ is the thickness of boundary layer momentum, and L/H is the of shock train length to isolator height ratio. The consistent coefficient (C) is defined for brevity targets. The amounts of L/H, θ/H and Re_θ are estimated 10, 0.02 and 10,000, respectively [30].

$$C = \frac{L}{H} \Big/ \frac{\sqrt{\theta/H}}{\sqrt[4]{\mathrm{Re}_\theta}} \tag{12.6}$$

The isolator exit pressure is defined by manipulating Eqs. (12.5) and (12.6) [30]:

$$P_C = P_B . \frac{\sqrt{680.C.\left(Ma_B^2 - 1\right) + 2500} + 290}{340} \tag{12.7}$$

The whole pressure and temperature at the isolator outlet are given as [29]:

$$T_{tC} = T_{tB} = T_{tA} \tag{12.8}$$

$$P_{tC} = P_C.\left(1 + (k-1).\frac{Ma_C^2}{2}\right)^{(k/k-1)} \tag{12.9}$$

$$\frac{P_{tC}}{P_{tB}} = \left[\left(\frac{1 + \frac{(k-1)}{2}.Ma_C^2}{1 + \frac{(k-1)}{2}.Ma_B^2}\right)^{(k/k-1)}\right].\left[\frac{1 + k.Ma_B^2}{1 + k.Ma_C^2}\right] \tag{12.10}$$

The static temperature at C is obtained from [29]:

$$T_C = T_{tC}/\left(1 + (k-1).\frac{Ma_C^2}{2}\right) \tag{12.11}$$

12.3.3.2 Heat Addition Process

Based on the energy conversation relation at steady state condition for the combustor, the Eq. (12.12) is written [30]:

$$\left(\dot{m}_A + \dot{m}_f\right)h_{tD} = \dot{m}_A h_{tC} + \dot{m}_f LHV_{H_2} \tag{12.12}$$

where, LHV_{H_2} is the hydrogen combustion low heat value and is reported 120.11 MJ/kg.

The Eq. (12.12) can be expressed in the other way as below:

$$\dot{m}_0 C_p T_{tC} + \dot{m}_f LHV_{H_2} = \dot{m}_0 C_p T_{tD} \tag{12.13}$$

or

$$\underset{f}{\dot{m}}\, LHV_{H_2} = \underset{A}{\dot{m}}\, C_p T_{tD}\left(T_{tC}/T_{tD} - 1\right) = \underset{A}{\dot{m}}\, C_p(T_{tD} - T_{tC}) \tag{12.14}$$

The whole temperature ratio is introduced as:

$$\tau = T_{tC}/T_{tD} \tag{12.15}$$

The stoichiometric hydrogen-air reaction is described as [33]:

$$2H_2 + O_2 + 3.76N_2 \rightarrow 2H_2O + 3.76N_2 \tag{12.16}$$

The highest demand of hydrogen $\dot{m}_{fs}$, takes place in the stoichiometric situation with Eq. (12.17):

$$\dot{m}_{fs} = \frac{\dot{m}_A \times 4 \times 0.21}{1 \times 32} \cong \dot{m}_A/40 \tag{12.17}$$

Also, the fuel equivalence ratio ($\varnothing$) is introduced as below:

$$\varnothing = \frac{\dot{m}_f}{\dot{m}_{fs}} \tag{12.18}$$

Moreover, the total temperature ratio may be described as below:

$$\tau = 1 + \frac{\varnothing LHV_{H_2}}{40 C_p T_{tA}} \tag{12.19}$$

In the constant pressure process:

$$P_D = P_C \tag{12.20}$$

Then, whole pressure P_{tD} is denoted as [29]:

$$P_{tD} = P_D.\left((k-1).\frac{Ma_D^2}{2} + 1\right)^{(k/k-1)} \tag{12.21}$$

$$\tau = \left[\frac{1 + k.Ma_C^2}{1 + k.Ma_D^2}\right].\left[\frac{Ma_D^2}{Ma_C^2}\right].\left[\left(\frac{1 + \frac{(k-1)}{2}.Ma_D^2}{1 + \frac{(k-1)}{2}.Ma_C^2}\right)^{(k/k-1)}\right] \tag{12.22}$$

By simultaneous solving of Eq. (12.21) and (12.22), the Mach number) and after that static temperature at the pint D are calculated.

$$T_D = T_{tD}/\left(1 + (k-1).\frac{Ma_D^2}{2}\right) \tag{12.23}$$

12.3.3.3 Expansion Process

Expansion process has been occurred isentropically in the nozzle as the followed relations [29]:

$$P_E = P_A \tag{12.24}$$

$$P_{tE} = P_{tD} \tag{12.25}$$

$$Ma_E = \sqrt{\left[\left(\frac{P_{tE}}{P_E}\right)^{(k-1/k)} - 1\right] \Big/ \left(\frac{k-1}{2}\right)} \tag{12.26}$$

12.3.4 Performance Criteria of Open Cooling Cycle

Decreasing in the fuel flow rate for refrigeration by rising the heat absorption of fuel is the prominent target of the OCC.

One of the main parameters is the multiplication ratio of the fuel heat absorption (δ), which is obtained from the first passage cooling per second passage cooling amounts as Eq. (12.27) [34].

$$\delta_1 = \frac{Q_2}{Q_1} \tag{12.27}$$

By the similar definition, δ_2, δ_3, and δ_4 are introduced for the third, fourth and fifth cooling passages, correspondingly:

$$\delta_2 = \frac{Q_3}{Q_1 + Q_2} \tag{12.28}$$

$$\delta_3 = \frac{Q_4}{Q_1 + Q_2 + Q_3} \tag{12.29}$$

$$\delta_4 = \frac{Q_5}{Q_1 + Q_2 + Q_3 + Q_4} \tag{12.30}$$

The other main parameter is introduced as reduction ratio of mass flow rate (ϕ). The increasing of the fuel heat absorption load is explained as decreasing in the mass flow rate of fuel. Particularly, direct effect of utilizing OCC in performance of the scramjet cooling unit is decreasing of the essential fuel flow rate. Moreover, the reduction ratio of the second cooling passage is described as below [34]:

$$\phi_1 = \frac{Q_2}{Q_1 + Q_2} \tag{12.31}$$

Similarly,ϕ_2, ϕ_3, and ϕ_4 are introduced for the third, fourth and fifth cooling passages, as written:

$$\phi_2 = \frac{Q_3}{Q_1 + Q_2 + Q_3} \tag{12.32}$$

$$\phi_3 = \frac{Q_4}{Q_1 + Q_2 + Q_3 + Q_4} \tag{12.33}$$

$$\phi_4 = \frac{Q_5}{Q_1 + Q_2 + Q_3 + Q_4 + Q_5} \tag{12.34}$$

12.3.5 PEM Electrolyzer Equations

The structure of PEM electrolyzer is drawn in the bottom section of Fig. 12.1. The main relations of the PEM set-up are described comprehensively in our other works [24, 35].

12.3.6 Thermodynamic Assessment

The governing format of the energy and mass balance at steady state condition may be explained as below [28, 36–38]:

$$\sum \dot{m}_{in} = \sum \dot{m}_{out} \tag{12.35}$$

$$\dot{Q} - \dot{W} = \sum \dot{m}_{out} h_{out} - \sum \dot{m}_{in} h_{in} \tag{12.36}$$

The energy performance of the suggested set-up is calculated from the summing the net generated power and produced hydrogen as products of the system divided by input heat as below:

$$\eta_{en} = \frac{(1 - \eta_G) \cdot \dot{W}_{net} + LHV_{H_2} \cdot \dot{m}_{15}}{\dot{Q}_{totla}} \tag{12.37}$$

where, $\dot{Q}_{total}$ is the scramjet's whole cooling utilized as the system heat source.

Some of the important thermodynamic relations which extracted from energy balance are tabulated in Table 12.1.

Total exergy rate ($\dot{E}x_{total}$) has four major part: physical exergy ($\dot{E}x_{PH}$), potential exergy ($\dot{E}x_{PT}$), kinetic exergy ($\dot{E}x_{KN}$), and chemical exergy rate ($\dot{E}x_{CH}$) [38, 39]:

$$\dot{E}x_{total} = \dot{E}x_{PH} + \dot{E}x_{PT} + \dot{E}x_{KN} + \dot{E}x_{CH} \tag{12.38}$$

Also, potential and kinetic exergies can be assumed negligible. The physical and chemical exergies are given as below [40]:

Table 12.1 Energy balance relations for each constituents of the recommended unit

Parameters	Relation
Power of turbine 1	$w_t = \eta_t c_p T_3 \left[1 - \pi_1^{(1-\gamma)/\gamma}\right]$
Power of pump	$w_p = \frac{P_2 - P_1}{\eta_p \rho_1}$
Whole net power	$w_{net} = w_{t1} + w_{t2} + w_{t3} + w_{t4} - w_p$
Net electricity	$\dot{W}_{net} = \dot{m}_0 w_{net}$
Cooling capacity of passage 1	$\dot{Q}_1 = \dot{m}_1 c_p (T_3 - T_2)$
Capacity of heat exchanger	$\dot{Q}_{HE} = \dot{m}_w (h_{13} - h_{12})$
Total cooling	$\dot{Q}_{total} = \dot{Q}_1 + \dot{Q}_2 + \dot{Q}_3 + \dot{Q}_4 + \dot{Q}_5 + \dot{Q}_{HE}$

$$\dot{E}x_{PH} = \dot{m}(h - h_0 - T_0(s - s_0)) \tag{12.39}$$

$$\dot{E}x_{CH} = \dot{m}\left[\sum_{i=1}^{n} y_i ex_{CH,i}^0 + RT_0 \sum_{i=1}^{n} y_i \mathbf{ln} y_i\right] \tag{12.40}$$

For each constituent, the exergy balance relation is denoted as [39, 41]:

$$\dot{E}x_F^i = \dot{E}x_P^i + \dot{E}x_D^i \tag{12.41}$$

In the above equation, $\dot{E}x_D^i$ is the exergy destruction, $\dot{E}x_P^i$ and $\dot{E}x_F^i$ are product and fuel exergies, respectively.

Exergetic efficiency of the constituents is written as:

$$\eta_{ex}^i = \dot{E}x_P^i / \dot{E}x_F^i \tag{12.42}$$

Destruction rate of each component can be expressed by exergy destruction ratio as below [39]:

$$Y_{D,i} = \dot{E}x_{D,i} / \dot{E}x_{D,total} \tag{12.43}$$

The overall exergetic efficiency of the set-up can be written as following

$$\eta_{ex}^{total} = \dot{E}x_P^{total} / \dot{E}x_F^{total} \tag{12.44}$$

Some of the necessary exergy relations of the recommended set-up is tabulated in Table 12.2

Table 12.2 Exergy equations of the main components of the simulated system

Component	Product exergy	Fuel exergy	Exergetic efficiency	Exergy destruction ratio
Turbine 1	$\dot{E}x_{P,t1} = \dot{W}_{t1}$	$\dot{E}x_{F,t1} = \dot{E}x_3 - \dot{E}x_4$	$\eta_{ex,t1} = \frac{\dot{E}x_{P,t1}}{\dot{E}x_{F,t1}}$	$Y_{D,t1} = \frac{\dot{E}x_{D,t1}}{\dot{E}x_{D,total}}$
Turbine 2	$\dot{E}x_{P,t2} = \dot{W}_{t2}$	$\dot{E}x_{F,t2} = \dot{E}x_5 - \dot{E}x_6$	$\eta_{ex,t2} = \frac{\dot{E}x_{P,t2}}{\dot{E}x_{F,t2}}$	$Y_{D,t2} = \frac{\dot{E}x_{D,t2}}{\dot{E}x_{D,total}}$
Turbine 3	$\dot{E}x_{P,t3} = \dot{W}_{t3}$	$\dot{E}x_{F,t3} = \dot{E}x_7 - \dot{E}x_8$	$\eta_{ex,t3} = \frac{\dot{E}x_{P,t3}}{\dot{E}x_{F,t3}}$	$Y_{D,t3} = \frac{\dot{E}x_{D,t3}}{\dot{E}x_{D,total}}$
Turbine 4	$\dot{E}x_{P,t4} = \dot{W}_{t4}$	$\dot{E}x_{F,t4} = \dot{E}x_9 - \dot{E}x_{10}$	$\eta_{ex,t4} = \frac{\dot{E}x_{P,t4}}{\dot{E}x_{F,t4}}$	$Y_{D,t4} = \frac{\dot{E}x_{D,t4}}{\dot{E}x_{D,total}}$
Cooling passage 1	$\dot{E}x_{P,CP1} = \dot{E}x_3 - \dot{E}x_2$	$\dot{E}x_{F,CP1} = \dot{Q}_1\left(1 - \frac{T_0}{T_{scr}}\right)$	$\eta_{ex,CP1} = \frac{\dot{E}x_{P,CP1}}{\dot{E}x_{F,CP1}}$	$Y_{D,CP1} = \frac{\dot{E}x_{D,CP1}}{\dot{E}x_{D,total}}$
Cooling passage 2	$\dot{E}x_{P,CP2} = \dot{E}x_5 - \dot{E}x_4$	$\dot{E}x_{F,CP2} = \dot{Q}_2\left(1 - \frac{T_0}{T_{scr}}\right)$	$\eta_{ex,CP2} = \frac{\dot{E}x_{P,CP2}}{\dot{E}x_{F,CP2}}$	$Y_{DCP2} = \frac{\dot{E}x_{D,CP2}}{\dot{E}x_{D,total}}$
Cooling passage 3	$\dot{E}x_{P,CP3} = \dot{E}x_7 - \dot{E}x_6$	$\dot{E}x_{F,CP3} = \dot{Q}_3\left(1 - \frac{T_0}{T_{scr}}\right)$	$\eta_{ex,CP3} = \frac{\dot{E}x_{P,CP3}}{\dot{E}x_{F,CP3}}$	$Y_{D,CP3} = \frac{\dot{E}x_{D,CP3}}{\dot{E}x_{D,total}}$
Cooling passage 4	$\dot{E}x_{P,CP4} = \dot{E}x_9 - \dot{E}x_8$	$\dot{E}x_{F,CP4} = \dot{Q}_4\left(1 - \frac{T_0}{T_{scr}}\right)$	$\eta_{ex,CP4} = \frac{\dot{E}x_{P,CP4}}{\dot{E}x_{F,CP4}}$	$Y_{D,CP4} = \frac{\dot{E}x_{D,CP4}}{\dot{E}x_{D,total}}$
Cooling passage 5	$\dot{E}x_{P,CP5} = \dot{E}x_{11} - \dot{E}x_{10}$	$\dot{E}x_{F,CP5} = \dot{Q}_5\left(1 - \frac{T_0}{T_{scr}}\right)$	$\eta_{ex,CP5} = \frac{\dot{E}x_{P,CP5}}{\dot{E}x_{F,CP5}}$	$Y_{D,CP5} = \frac{\dot{E}x_{D,CP5}}{\dot{E}x_{D,total}}$
PEM	$\dot{E}x_{P,PEM} = \dot{E}x_{14} + \dot{E}x_{15}$	$\dot{E}x_{F,PEM} = (1 - \eta_G)\dot{W}_{net}$	$\eta_{ex,PEM} = \frac{\dot{E}x_{P,PEM}}{\dot{E}x_{F,PEM}}$	$Y_{D,PEM} = \frac{\dot{E}x_{D,PEM}}{\dot{E}x_{D,total}}$
Pump	$\dot{E}x_{P,p} = \dot{E}x_2 - \dot{E}x_1$	$\dot{E}x_{F,p} = \dot{W}_p$	$\eta_{ex,p} = \frac{\dot{E}x_{P,p}}{\dot{E}x_{F,p}}$	$Y_{D,p} = \frac{\dot{E}x_{D,p}}{\dot{E}x_{D,total}}$
Heat exchanger	$\dot{E}x_{P,HE} = \dot{E}x_{13} - \dot{E}x_{12}$	$\dot{E}x_{F,HE} = \dot{Q}_{HE}\left(1 - \frac{T_0}{T_{scr}}\right)$	$\eta_{ex,HE} = \frac{\dot{E}x_{P,HE}}{\dot{E}x_{F,HE}}$	$Y_{D,HE} = \frac{\dot{E}x_{D,HE}}{\dot{E}x_{D,total}}$

12.3.7 Multi-criteria Optimization

In this investigation, optimization procedure is applied to maximize the energy and exergy efficiencies simultaneously. The multi-criteria optimization procedure is utilized via genetic algorithm (GA) which is a strong approach compared to other methods [42].

Two Thermodynamics factor, consisting of the energy and exergy efficiencies have been determined as objective functions, while the six parameters are presented as the prominent decision variables. The multi-criteria function is presented in Eq. (12.45), and the major target of optimization is maximizing the suggested function.

$$Max(MCF = w_1 \times \eta_{en} + w_2 \times \eta_{ex}), \tag{12.45}$$

$$w_1 + w_2 = 1, 0 \leq w_1, w_2 \leq 1$$

$$200 \leq T_1(K) \leq 250$$

$$200 \leq T_{15}(K) \leq 250$$

$$0.1 \leq P_1(MPa) \leq 0.4 \tag{12.46}$$

$$15 \leq P_2(MPa) \leq 25$$

$$5 \leq Mach_A \leq 7$$

$$0.5 \leq \eta_G \leq 0.7$$

Moreover, Table 12.3 shows some main accountable parameters applied in the GA.

Table 12.3 Some main accountable parameters applied in the GA [43–46]

Parameter	Value
Individuals population number	32
Generation number	64
Highest mutation rate	0.25
Lowest mutation rate	0.0005
Crossover probability	0.85
Primary mutation rate	0.25

12.4 Result and Arguments

Based on coding in EES software, the recommended set-up is analyzed from energy and exergy standpoint. Table 12.4 expressed the initial parameters for modeling the set-up. The calculated outcomes regarding to prominent thermodynamic flow properties are written in Table 12.5. The properties consist of pressure, temperature, mass flow rate, enthalpy, entropy, and exergy rate at each state.

12.4.1 Results of Thermodynamic Simulation

This section reveals the results of simulation, in which 4840 kW and 59.45 kg/h power and hydrogen are produced and 13.87% total energy efficiency is achieved for uniform condition of $m = 0.4$ kg/s, $Ma_A = 6$, $T_A = 223$ K, $P_A = 2.56$ kPa when 65% of the generated electricity is consumed in the PEM electrolyzer. The quantity of hydrogen production is satisfying compared to that of other similar systems, which can be widely used in aerospace industry (Table 12.6).

Table 12.7 and Fig. 12.4 demonstrate the results of exergy analysis. Accordingly, the overall exergy efficiency is 17.48%, and the PEM electrolyzer and the first cooling pas-sage account for the highest exergy destruction, with 72.47% and 10.67%

Table 12.4 Input data for simulation of the set-up

Parameter	Value
Efficiency of Generator power, η_G	0.65
Efficiency of pump, η_p	0.7
Efficiency of turbine, η_t	0.8
Temperature of PEM, T_{PEM} (K)	353
Temperature of PEM entrance water, T_{12} (K)	298
PEM entrance water mass flow rate, $\dot{m}_{12}$ (kg/s)	0.0311
Fuel mass flow rate, $\dot{m}_0$ (kg/s)	0.4
Pressure of fuel tank, P_1 (MPa)	0.24
Temperature of fuel tank, T_1 (K)	225
Pressure of Scramjet combustion chamber, P_{11} (MPa)	1
Pump's back pressure, P_2 (MPa)	22
Ratio of inlet pressure, π_{in}	300
Ratio of fuel equivalence, $\varnothing$	0.6
Temperature of Freestream, TA (K)	223
Pressure of Freestream, P_A (MPa)	0.00256
Mach number of Freestream, Ma_A	6

Table 12.5 Thermodynamic properties in each state of the set-up

State	Fluid	T (K)	P (MPa)	$\dot{m}$ (kg/s)	h (kJ/kg)	s (kJ/kg.K)	$\dot{E}x$ (kW)
1	H_2	225	0.24	0.4	617.1	57.22	509.3
2	H_2	254.9	22	0.4	1037	57.22	677.3
3	H_2	1408	22	0.4	16,555	65.46	6590
4	H_2	1006	4.69	0.4	10,349	66.66	3969
5	H_2	1408	4.69	0.4	16,555	71.84	5850
6	H_2	1185	2.166	0.4	13,073	72.33	4400
7	H_2	1408	2.166	0.4	16,555	75.02	5481
8	H_2	1291	1.472	0.4	14,706	75.25	4715
9	H_2	1408	1.471	0.4	16,555	76.62	5296
10	H_2	1291	1	0.4	14,706	76.84	4530
11	H_2	1408	1	0.4	16,555	78.21	5111
12	H_2O	290	0.101	0.0321	70.75	0.251	83.53
13	H_2O	353	0.101	0.0321	334.3	1.073	84.33
14	O_2	353	0.101	0.0929	50.36	0.156	31.27
15	H_2	353	0.101	0.01171	789.3	67.21	3.357

proportional exergy destruction ratio caused by chemical reaction and high temperature difference, respectively [47]. There is a direct relation between the temperature difference and exergy destruction [39]. Also, the highest exergy efficiency belongs to the pump in the system.

12.4.2 Optimization Results

In this section, optimized outcomes are reported and the comparison be-tween base scenario and multi-criteria optimizing scenario (MCO) have been presented in the Fig. 12.5. Accordingly, the energy efficiency increases from 13.87% to 20.7% (49.24% improvement) and exergy efficiency rises from 17.87% to 26.09% (45.98% improvement). Also. The last column of the results shows the optimized amounts of decision variables.

12.5 Noteworthy Conclusions

In our previous work [19] a novel M-OCC system is proposed and its analytic modeling developed. The previous study showed that the proposed system not only is able to aid scramjet in managing the heat properly but also has great potential in producing other variant useful energy forms such as electric power and hydrogen as

Table 12.6 The outcomes of the energy assessment

Parameter	Amount
Pump power, w_p (MJ/kg)	0.4353
Net electricity output, $\dot{W}_{net}$ (kW)	4840
Power of turbine 1, w_{t1} (MJ/kg)	5.856
power of turbine 2, w_{t2} (MJ/kg)	3.25
power of turbine 3, w_{t3} (MJ/kg)	1.715
power turbine 4, w_{t4} (MJ/kg)	1.715
Total cooling, $\dot{Q}_{total}$(kW)	12,231
PEM power entrance, $\dot{W}_G$ (kW)	3146
PEM heat exchanger load, $\dot{Q}_{HE}$ (kW)	8.461
Hydrogen production, $\dot{m}_{H_2}$ (kg/h)	59.45
heat load in cooling passage I, $\dot{Q}_1$ (kW)	6869
heat load in cooling passage II, $\dot{Q}_2$ (kW)	2482
heat load in cooling passage III, $\dot{Q}_3$ (kW)	1393
heat load in cooling passage IV, $\dot{Q}_4$ (kW)	739.6
heat load in cooling passage V, $\dot{Q}_5$ (kW)	739.6
Reduction ratio II, ϕ_1	0.2585
Reduction ratio III, ϕ_2	0.08025
Reduction ratio IV, ϕ_3	0.03107
Reduction ratio V, ϕ_4	0.03106
Energy efficiency overall system, η_{en} (%)	13.87
Multiplication ratio II, δ_1	0.3487
Multiplication ratio III, δ_2	0.1189
Multiplication ratio IV, δ_3	0.04234
Multiplication ratio V, δ_4	0.04232
Average temperature of scramjet combustion chamber, T_{ave} (K)	1408
Reduction ratio II, ϕ_1	0.2585
Reduction ratio III, ϕ_2	0.08025
Reduction ratio IV, ϕ_3	0.03107
Reduction ratio V, ϕ_4	0.03106

fuel, by recovering a useless waste heat. Accordingly, the necessity of conducting a research work to improve the performance of the proposed system is comprehensible. Thus the present study focused on the optimization of novel M-OCC system. The present study had been accomplished to have a better understanding from the system's operation. The following outlines can be expressed as brief:

- The energy efficiency of the system have been increased from 13.87 to 20.7%.
- The exergy efficiency of the system have been increased from 17.87 to 26.09%.

Table 12.7 Exergy results of the equipment

Sector	$\dot{E}x_F$(kW)	$\dot{E}x_P$(kW)	$\dot{E}x_D$(kW)	η_{ex}(%)	Y_D(%)
Cooling passage I	5912	5485.4	458.2	92.25	10.67
Cooling passage II	1971	1881	89.91	95.43	2.094
Cooling passage III	1106	1081	25.33	97.6	0.59
Cooling passage IV	587.3	580.6	6.729	98.85	0.1567
Cooling passage V	587.3	580.6	6.729	98.85	0.1567
Pump	174.1	168	6.172	96.46	0.1438
Turbine 1	2620	2342	278.1	87	6.47
Turbine 2	1450	1300	150.3	89.39	3.5
Turbine 3	765.4	685.8	79.59	89.63	1.85
Turbine 4	765.4	685.8	79.59	89.6	1.85
PEM heat exchanger	1.883	0.8046	1.078	42.74	0.0251
PEM	3146	34.63	3111	1.101	72.47
Total	9708	1697	4293	17.87	–

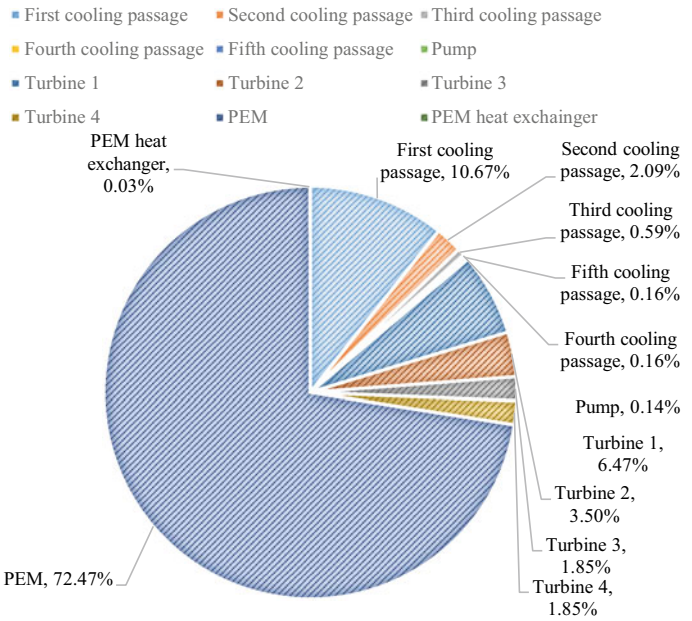

Fig. 12.4 Diagram of exergy destruction in different fixtures of the system

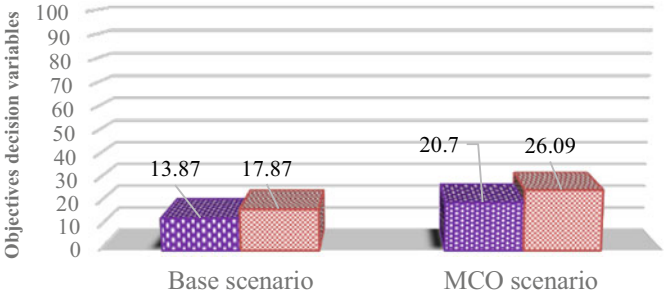

w_1	-	1/2
w_2	-	1/2
$T_1(K)$	225	249.7
$T_{15}(K)$	353	355.1
$P_1(MPa)$	0.24	0.201
$P_2(MPa)$	22	25
$Mach_A$	6	5.797
η_G	0.65	0.512

Fig. 12.5 Comparison of major parameters for base and optimum scenarios

- The overall improvement of the system performance is more than 45% which is really considerable.

References

1. W.H. Heiser, D.T. Pratt, *Hypersonic airbreathing propulsion* (Aiaa, 1994.), vol. 1
2. E.T. Curran, Scramjet engines: The first forty years. J. Propul. Power **17**(6), 1138–1148 (2001)
3. P.L. Moses et al., NASA hypersonic flight demonstrators—Overview, status, and future plans. Acta Astronaut. **55**(3–9), 619–630 (2004)
4. R. Varvill, A. Bond, A comparison of propulsion concepts for SSTO reusable launchers. J. Br. Interplanet. Soc. **56**(3/4), 108–117 (2003)
5. X. Li, Z. Wang, Exergy analysis of integrated TEG and regenerative cooling system for power generation from the scramjet cooling heat. Aerosp. Sci. Technol. **66**, 12–19 (2017)
6. E. Daniau, et al., Fuel reforming for scramjet thermal management and combustion optimization, in *AIAA/CIRA 13th International Space Planes and Hypersonics Systems and Technologies Conference*, 2005
7. W. Bao et al., Effect of cooling channel geometry on re-cooled cycle performance for hydrogen fueled scramjet. Int. J. Hydrogen Energy **35**(13), 7002–7011 (2010)
8. W. Bao et al., Power generation and heat sink improvement characteristics of recooling cycle for thermal cracked hydrocarbon fueled scramjet. Sci. China Technol. Sci. **54**(4), 955–963 (2011)

9. H. Nasrollahi, et al., The greenhouse technology in different climate conditions: A comprehensive energy-saving analysis. Sustain. Energy Technol. Assessm. **47**, 101455 (2021)
10. H. Cho, A.D. Smith, P. Mago, Combined cooling, heating and power: A review of performance improvement and optimization. Appl. Energy **136**, 168–185 (2014)
11. M. Mohsenipour et al., Investigation of a geothermal-based CCHP system from energetic, water usage and CO_2 emission viewpoints. Gas Process. J. **7**(1), 41–52 (2019)
12. L. Jiang et al., Experimental study on a resorption system for power and refrigeration cogeneration. Energy **97**, 182–190 (2016)
13. T. Ratlamwala, I. Dincer, Comparative efficiency assessment of novel multi-flash integrated geothermal systems for power and hydrogen production. Appl. Therm. Eng. **48**, 359–366 (2012)
14. F. Sun et al., New waste heat district heating system with combined heat and power based on absorption heat exchange cycle in China. Appl. Therm. Eng. **37**, 136–144 (2012)
15. H. Onovwiona, V.I. Ugursal, Residential cogeneration systems: Review of the current technology. Renew. Sustain. Energy Rev. **10**(5), 389–431 (2006)
16. M.S. Azhar, G. Rizvi, I. Dincer, Integration of renewable energy based multigeneration system with desalination. Desalination **404**, 72–78 (2017)
17. H. Ghaebi, H. Rostamzadeh, P.S. Matin, Performance evaluation of ejector expansion combined cooling and power cycles. Heat Mass Transf. **53**(9), 2915–2931 (2017)
18. A.R. Choudhuri, S. Gollahalli, Combustion characteristics of hydrogen–hydrocarbon hybrid fuels. Int. J. Hydrogen Energy **25**(5), 451–462 (2000)
19. P. Seyedmatin, et al., Electricity and hydrogen co-production via scramjet multi-expansion open cooling cycle coupled with a PEM electrolyzer. Energy **199**, 117364 (2020)
20. M. Carmo et al., A comprehensive review on PEM water electrolysis. Int. J. Hydrogen Energy **38**(12), 4901–4934 (2013)
21. M. Lebbal, S. Lecœuche, Identification and monitoring of a PEM electrolyser based on dynamical modelling. Int. J. Hydrogen Energy **34**(14), 5992–5999 (2009)
22. F. Marangio, M. Santarelli, M. Calì, Theoretical model and experimental analysis of a high pressure PEM water electrolyser for hydrogen production. Int. J. Hydrogen Energy **34**(3), 1143–1158 (2009)
23. P. Ahmadi, I. Dincer, M.A. Rosen, Energy and exergy analyses of hydrogen production via solar-boosted ocean thermal energy conversion and PEM electrolysis. Int. J. Hydrogen Energy **38**(4), 1795–1805 (2013)
24. M. Ebadollahi et al., Proposal and assessment of a new geothermal-based multigeneration system for cooling, heating, power, and hydrogen production, using LNG cold energy recovery. Renew. Energy **135**, 66–87 (2019)
25. A. Pirmohamadi et al., Exergoeconomic analysis of a novel hybrid system by integrating the kalina and heat pump cycles with a nitrogen closed brayton system. Energy Rep. **7**, 546–564 (2021)
26. M. Ebadollahi, et al., Thermal and exergetic performance enhancement of basic dual-loop combined cooling and power cycle driven by solar energy. Therm. Sci. Eng. Progress **18**, 100556 (2020)
27. M. Mohsenipour, et al., Design and evaluation of a solar-based trigeneration system for a nearly zero energy greenhouse in arid region. J. Clean. Prod. **254**, 119990 (2020)
28. H. Rostamzadeh et al., Energy and exergy analysis of novel combined cooling and power (CCP) cycles. Appl. Therm. Eng. **124**, 152–169 (2017)
29. J.D. Anderson, *Modern Compressible Flow: With Historical Perspective* (McGraw-Hill, New York, 1990), vol. 2
30. Q. Yang, J. Chang, W. Bao, Thermodynamic analysis on specific thrust of the hydrocarbon fueled scramjet. Energy **76**, 552–558 (2014)
31. F.S. Billig, Research on supersonic combustion. J. Propul. Power **9**(4), 499–514 (1993)
32. P. Waltrup, F.S. Billig, Prediction of precombustion wall pressure distributions in scramjet engines. J. Spacecr. Rocket. **10**(9), 620–622 (1973)
33. J.W. Heffel, NOx emission and performance data for a hydrogen fueled internal combustion engine at 1500rpm using exhaust gas recirculation. Int. J. Hydrogen Energy **28**(8), 901–908 (2003)

34. J. Qin et al., Performance cycle analysis of an open cooling cycle for a scramjet. Proc. Inst. Mech. Eng. Part G J. Aerosp. Eng. **223**(6), 599–607 (2009)
35. M. Ebadollahi et al., Energy and Exergy Analysis of a Geothermal-Based Multi-generation System, in *Integration of Clean and Sustainable Energy Resources and Storage in Multi-Generation Systems.* (Springer, 2020), pp. 121–140
36. Y.A. Cengel, M.A. Boles, Thermodynamics: An engineering approach. Sea **1000**, 8862 (2002)
37. M. Bezaatpour et al., Magnetic-induced nanoparticles and rotary tubes for energetic and exergetic performance improvement of compact heat exchangers. Powder Technol. **377**, 396–414 (2021)
38. M.-R. Kolahi, M. Amidpour, M. Yari, Multi-objective metaheuristic optimization of combined flash-binary geothermal and humidification dehumidification desalination systems. Desalination **490**, 114456 (2020)
39. A. Bejan, G. Tsatsaronis, *Thermal Design and Optimization* (John Wiley & Sons, 1996)
40. R. Kheiri et al., Thermodynamic modeling and performance analysis of four new integrated organic Rankine cycles (A comparative study). Appl. Therm. Eng. **122**, 103–117 (2017)
41. M. Kolahi et al., Thermodynamic and economic performance improvement of ORCs through using zeotropic mixtures: Case of waste heat recovery in an offshore platform. Case Stud. Therm. Eng. **8**, 51–70 (2016)
42. H. Rostamzadeh, et al., Exergoeconomic optimisation of basic and regenerative triple-evaporator combined power and refrigeration cycles. **26**(1–2), 186–225 (2018)
43. M. Ebadollahi, et al., Close supercritical versus inverse brayton cycles for power supply, using waste of a biogas-driven open brayton cycle. J. Energy Resour. Technol. **143**(9) (2021)
44. M. Ebadollahi et al., Proposal and multi-criteria optimization of two new combined heating and power systems for the Sabalan geothermal source. J. Clean. Prod. **229**, 1065–1081 (2019)
45. M. Ebadollahi et al., Exergoeconomic analysis and optimization of innovative cascade bi-evaporator electricity/cooling cycles with two adjustable cooling temperatures. Appl. Therm. Eng. **152**, 890–906 (2019)
46. H. Rostamzadeh et al., Comparative study of two novel micro-CCHP systems based on organic Rankine cycle and Kalina cycle. Energy Convers. Manage. **183**, 210–229 (2019)
47. T.J. Kotas, *The Exergy Method of Thermal Plant Analysis* (Elsevier, 2013)